Sciencexpress Reports

Conformational plasticity of a native retroviral capsid revealed by x-ray crystallography

G. Obal,[1,2]* F. Trajtenberg,[3]* F. Carrión,[1] L. Tomé,[1,2]† N. Larrieux,[3] X. Zhang,[4] O. Pritsch,[1,2]‡ A. Buschiazzo[3,5]‡

[1]Institut Pasteur de Montevideo, Unit of Protein Biophysics, Mataojo 2020, 11400, Montevideo, Uruguay. [2]Departamento de Inmunobiología, Facultad de Medicina, Universidad de la República, Avenida General Flores 2125, 11800, Montevideo, Uruguay. [3]Institut Pasteur de Montevideo, Unit of Protein Crystallography, Mataojo 2020, 11400, Montevideo, Uruguay. [4]Institut Pasteur, Unité de Virologie Structurale, Département de Virologie and CNRS Unité Mixte de Recherche 3569, 28, Rue du Dr Roux, 75015, Paris, France. [5]Institut Pasteur, Department of Structural Biology and Chemistry, 25, Rue du Dr Roux, 75015, Paris, France.

*These authors contributed equally to this work.

†Present address: Institut Pasteur, Viruses and RNA interference Unit and Centre National de la Recherche Scientifique, UMR 3569, 28, Rue du Dr Roux, 75015, Paris, France.

‡Corresponding author. E-mail: pritsch@pasteur.edu.uy (O.P.); alebus@pasteur.edu.uy (A.B.)

Retroviruses depend upon self-assembly of their capsid proteins (core particle) to yield infectious mature virions. Despite the essential role of the retroviral core, its high polymorphism has hindered high-resolution structural analyses. Here, we report the x-ray structure of the native capsid (CA) protein from bovine leukemia virus. CA is organized as hexamers that deviate significantly from 6-fold symmetry, yet adjust to make two-dimensional pseudo-hexagonal arrays that mimic mature retroviral cores. Intra- and interhexameric quasi-equivalent contacts are uncovered, with flexible trimeric lateral contacts among hexamers, yet preserving very similar dimeric interfaces making the lattice. The conformation of each capsid subunit in the hexamer is therefore dictated by long-range interactions, revealing how the hexamers can also assemble into closed core particles, a relevant feature of retrovirus biology.

Retroviruses undergo an obligatory maturation step in the formation of infectious particles (*1*–*3*). The cleavage of Gag generates several mature proteins, including capsid (CA), which self-assembles into a fullerene-like core, enclosing the RNA genome. Revealing the molecular features of the retroviral mature core and its assembly mechanism is important for understanding retrovirus biology and developing novel antiretroviral drugs.

Retroviral cores display variable shapes and sizes (*4*, *5*), sharing a similar organization into a fullerene-like array of hexameric CA building units, with 12 interspersed CA pentamers to allow for particle closure (*6*, *7*). The CA protomer is composed of two α-helical domains, N- and C-terminal (NTD and CTD) (*8*–*11*), connected by a flexible linker (*2*). The crystal structure of the intact CA molecule has been challenging because of its intrinsic flexibility (*12*–*15*) and tendency to self-assemble into heterogenous structures. Stabilization of HIV-1 CA hexamer and pentamer building units by cysteine engineering, eventually lead to solving their crystal structures (*14*, *16*), albeit including additional mutations that destabilize critical contacts. Together with state-of-the-art cryoEM analyses of tubular assemblies of native HIV-1 CA (*17*, *18*), unprecedented insight into the architecture of the core particle has been provided, extending earlier lower resolution studies (*19*): a central 5-fold or 6-fold symmetric, seemingly rigid ring of NTDs, is surrounded by an outer belt of mobile CTDs, involved in lateral CTD-CTD dimer contacts among hexamers to form the fullerene lattice (*14*). Trimeric CTD interfaces, observed only in tubular assemblies, have been proposed to play a key role for lattice curvature (*17*, *18*).

We now report the crystal structure of the native, mature CA protein from bovine leukemia virus (BLV) at 2.75Å resolution. A tumorigenic B-lymphotropic Deltaretrovirus, BLV infects cattle worldwide (*20*–*22*) and is closely related to human T-lymphotropic viruses (HTLV) (*23*). BLV CA (Fig. 1A) crystallized in space group $P6_5$, with one hexamer in the asymmetric unit (Fig. 1B) and a similar overall architecture as HIV-1 CA (*14*). However, the BLV CA hexamer deviates substantially from 6-fold symmetry, yet able to make a flat pseudo-hexagonal lattice (Fig. 1C). The 6_5 screw axis relates successive layers along the c axis of the crystal (fig. S1), with the quasi 6-fold (Q6) axis of the hexamer off-centered from the crystallographic one, and tilted by approximately 7 degrees (Fig. 1D and fig. S1). The structures of the individual NTD and CTD subdomains of BLV CA were determined, respectively to 1.44 and 2.45 Å resolution (table S1 and fig. S2), which was instrumental in the structure determination process (*24*). The NTD and CTD structures are organized as their counterparts in other retroviruses (fig. S3), displaying highest similarity to HTLV-1 (table S2).

The BLV CA hexamer is stabilized through two types of interfaces (Fig. 2), NTD-NTD and NTD-CTD, as in other retroviral CA proteins (*11*, *14*, *18*, *25*). The core of the inner NTD ring is formed by the first three α-helices of each protomer, packed together through van der Waals interactions, with buried surfaces ranging from 360Å^2 to 460Å^2 for each

protomer at the six NTD-NTD interfaces (Fig. 2B). Two hydrogen bonds were also consistently observed (Fig. 2B), with one or two additional H-bonds present only in some pairs. Water-mediated hydrogen bonds could not be satisfactorily modeled at this resolution. On the other hand, NTD-CTD intra-hexamer contacts were observed both within and between protomers. Intra-protomer contacts associate helices α2 and α7 of the NTD, with CTD α8 and the α8-α9 loop, burying 280-300 Å^2. Inter-protomer NTD-CTD interactions (Fig. 2C) involve NTD α4 and CTD α8 and α11, burying areas of 280 Å^2 to 400 Å^2 per protomer. All interfaces are thus relatively small, consistent with the large variation found in the relative positioning of the various pairs of interacting protomers (Fig. 2, B and C), related to the imperfect Q6 symmetry of the hexamer (Fig. 1B).

Comparison of the crystallized hexamer with the closest 6-fold symmetrized hexamer (*24*) yielded a rather high rmsd of 2.8 Å (for 1136 Cα superposed atoms). Moreover, symmetrizing the NTD and CTD rings separately, resulted in rmsds of 2.4 Å and 1.9 Å (732 and 420 Cα superposed atoms, respectively), relative to their counterparts in the crystal structure. These deviations from strict C_6 (proper 6-fold rotational) symmetry indicate that the CA hexamer is plastic, giving rise to both intra- (fig. S4) and inter-capsomer (fig. S1C) quasi-equivalent protein contact interfaces.

In the planar lattice of the crystals, the tilt of the Q6 axis of the hexamer with respect to the crystal c axis results in a tiled pattern of juxtaposed hexamers in one direction (Fig. 1D). The packing is such that it gives rise to three independent quasi-2-fold (Q2) and two quasi-3-fold (Q3) lateral contacts (Fig. 1C), fitting adjacent hexamers tightly together along continuous planes (fig. S5). The CTD "dimers" related by the 3 independent Q2 axes are very similar to each other (fig. S6), involving mainly hydrophobic packing of the 3_{10} helix, the α8-α9 loop and helix α9. The side chains of residues Trp133 (within the 3_{10} helix) and Ile168 (in α9) play prominent roles, resembling the geometry observed in the crystal structures of the isolated HIV-1 CTD dimer (*26*). Buried interface areas at the BLV Q2 axes vary between 440Å^2 and 550Å^2 per protomer, comparable to the single dyad in HIV-1 structures and displaying an overall similar arrangement (*14*, *27*). The Trp133/Ile168 pair (fig. S6) plays an analogous role as Trp184/Met185 of HIV-1, suggesting a functional conservation of these hydrophobic residues. Similarly, the pair Val163/Pro164 in BLV, occupies an equivalent position to HIV-1 Val181. Residues located at different secondary structure elements, direct their side chains to occupy matching volumes in space, docking the CTD dimer unit in a conserved way.

The two independent Q3 contacts, in contrast to the Q2 interfaces, are quite different to each other (Fig. 3). They engage equivalent interaction surfaces as observed in HIV CA tubes (*17*), encompassing helices α10 and α11 of the three CTDs. Several side chains at the Q3 interfaces in BLV CA display weak electron density, indicating relative mobility of these residues. The surfaces contributed by chains A-C-E at one of the Q3 axes, bury areas of 460 Å^2, 360 Å^2 and 325 Å^2, respectively; whereas the B-D-F interface buries 375 Å^2, 200 Å^2 and 350 Å^2. Residues at the C terminus of α10, mainly Gln186-Gly187-Arg188, together with residues from α11, make loose interactions among the three contacting CTDs. The Q3 interfaces seem remarkably supple, consistent with the large variations among the equivalent contact areas present in HIV-1 CA tubes (*17*) as well as the shifts observed in dehydrated HIV-1 CA crystals (*27*). Moreover, the 3-fold interfaces are not restricted to curved lattices, in contrast to previous suggestions (*17*), since they are present in the planar lattice of BLV CA involving comparable interface areas as the dimeric ones. The 2D hexagonal arrays in the P6 structures of HIV-1 CA are stabilized via dimer CTD contacts, with no protein interactions on the 3-fold axes (fig. S5), yet the latter do show key interactions in tubular HIV-1 CA assemblies (*17*, *18*). The P6 crystal packing may thus be favoring a symmetric organization at the expense of lateral contacts. Altogether, a snug fit among hexamers with simultaneous 2-fold and 3-fold contacts, appears to be linked to global asymmetry in the forms of capsomer deformation or 2D lattice curvature.

To gain further functional insights of CA plasticity, we studied in vitro the self-assembly of full-length BLV CA, comparing the mature form (used to crystallize) to a variant mimicking the immature state. The latter included one additional N-terminal residue coming from Gag, expected to disrupt the N-terminal β-hairpin of mature CA. While the mature form generated large 2D sheets, consistent with the planar layers observed in the crystal structure, the one lacking the β-hairpin exclusively made tubular assemblies (fig. S7). To understand the striking difference, we attempted crystallization of the immature variant, and obtained crystals only for the isolated NTD (termed NTD-nobeta, table S1). The crystal structure revealed no electron density for the N-terminal segment (amino acids 1-11), indicating that these residues are disordered in the absence of β-hairpin formation. It has been postulated that β-hairpin formation upon the maturation cleavage of Gag could be linked to structural rearrangements of helix α1 (*28*, *29*), eventually favoring formation of the mature CA hexamer. Comparing the NTD structures of BLV with and without β-hairpin, a significant shift of helix α1 was indeed observed (fig. S8).

The range of different NTD-NTD and NTD-CTD orientations within the hexamer (Fig. 2) provides a connected network for the propagation of long-range forces. Modifications at the NTD correlate with lattice modulation (figs. S7 and S8), even if NTDs are not in direct contact among adjacent hexameric units. Similar observations with HIV-1 CA (*30*) are consistent with this hypothesis. By binding small molecules (*27*, *31*) or protein partners (*32*) in the infected cell, NTDs could induce CTD-CTD interface rearrangements deeper within the core, ultimately modulating capsid stability.

In conclusion, we have now captured the natural plasticity of the retroviral capsid assembly unit by working with a CA protein with no engineered mutations. With one hexamer in the asymmetric unit, no crystallographic symmetry constraint is imposed onto individual protomers. Our structure provides a snapshot of one asymmetric conformation, probably among different ones accessible to the hexameric unit. The simplest packing of hexamers into a planar lattice would be a truly symmetric honeycomb array, as observed in the layers of the P6 crystals from HIV-1 CA (*14*). Such a packing is obviously not favored for BLV CA, likely due to non-optimal interacting surfaces for hexamers to pile directly on top of each other. Yet the BLV CA hexamer finds a way to pack in 2D sheets by shifting laterally and tilting from the crystal c axis. The constrain of building layers to form a $P6_5$ crystal leads to the deformation of the ring such that non-identical Q2 and Q3 lateral contacts of tilted hexamers result in a planar lattice. This is a demonstration of the striking ability of the CA protein to conform to long-range interactions, and provides insight on how closure of the CA core may be linked to the actual conformation of the individual hexamers. It also sheds new light into the observed polymorphism of retrovirus mature cores in general. In contrast with the current paradigm, which states that the CTDs in the outer ring adapt to different packing environments by altering their relations to the inner, rigid NTD ring (*14*, *17*), we now observe that the inner NTD ring is also plastic, deviating substantially from a symmetric configuration in order to conform to the dominant long-range interactions. This model of capsid plasticity contributes with a novel framework to develop more accurate hypotheses of capsid self-assembly and uncoating. Implications of this mechanism seem relevant for the discovery of allosteric effectors with novel antiretroviral properties.

REFERENCES AND NOTES

1. J. A. Briggs, H. G. Kräusslich, The molecular architecture of HIV. *J. Mol. Biol.* **410**, 491–500 (2011). Medline doi:10.1016/j.jmb.2011.04.021
2. B. K. Ganser-Pornillos, M. Yeager, O. Pornillos, Assembly and architecture of HIV. *Adv. Exp. Med. Biol.* **726**, 441–465 (2012). Medline
3. F. K. Schur, W. J. H. Hagen, M. Rumlová, T. Ruml, B. Müller, H.-G. Kräusslich, J. A. G. Briggs, Structure of the immature HIV-1 capsid in intact virus particles at 8.8 Å resolution. *Nature* **517**, 505–508 (2014). Medline doi:10.1038/nature13838
4. B. K. Ganser-Pornillos, U. K. von Schwedler, K. M. Stray, C. Aiken, W. I. Sundquist, Assembly properties of the human immunodeficiency virus type 1 CA protein. *J. Virol.* **78**, 2545–2552 (2004). Medline doi:10.1128/JVI.78.5.2545-2552.2004
5. J. Benjamin, B. K. Ganser-Pornillos, W. F. Tivol, W. I. Sundquist, G. J. Jensen, Three-dimensional structure of HIV-1 virus-like particles by electron cryotomography. *J. Mol. Biol.* **346**, 577–588 (2005). Medline doi:10.1016/j.jmb.2004.11.064
6. S. Li, C. P. Hill, W. I. Sundquist, J. T. Finch, Image reconstructions of helical assemblies of the HIV-1 CA protein. *Nature* **407**, 409–413 (2000). Medline doi:10.1038/35030177
7. B. K. Ganser, S. Li, V. Y. Klishko, J. T. Finch, W. I. Sundquist, Assembly and analysis of conical models for the HIV-1 core. *Science* **283**, 80–83 (1999). Medline doi:10.1126/science.283.5398.80
8. R. K. Gitti, B. M. Lee, J. Walker, M. F. Summers, S. Yoo, W. I. Sundquist, Structure of the amino-terminal core domain of the HIV-1 capsid protein. *Science* **273**, 231–235 (1996). Medline doi:10.1126/science.273.5272.231
9. T. R. Gamble, S. Yoo, F. F. Vajdos, U. K. von Schwedler, D. K. Worthylake, H. Wang, J. P. McCutcheon, W. I. Sundquist, C. P. Hill, Structure of the carboxyl-terminal dimerization domain of the HIV-1 capsid protein. *Science* **278**, 849–853 (1997). Medline doi:10.1126/science.278.5339.849
10. C. C. Cornilescu, F. Bouamr, X. Yao, C. Carter, N. Tjandra, Structural analysis of the N-terminal domain of the human T-cell leukemia virus capsid protein. *J. Mol. Biol.* **306**, 783–797 (2001). Medline doi:10.1006/jmbi.2000.4395
11. G. B. Mortuza, L. F. Haire, A. Stevens, S. J. Smerdon, J. P. Stoye, I. A. Taylor, High-resolution structure of a retroviral capsid hexameric amino-terminal domain. *Nature* **431**, 481–485 (2004). Medline doi:10.1038/nature02915
12. S. Khorasanizadeh, R. Campos-Olivas, M. F. Summers, Solution structure of the capsid protein from the human T-cell leukemia virus type-I. *J. Mol. Biol.* **291**, 491–505 (1999). Medline doi:10.1006/jmbi.1999.2986
13. R. Campos-Olivas, J. L. Newman, M. F. Summers, Solution structure and dynamics of the Rous sarcoma virus capsid protein and comparison with capsid proteins of other retroviruses. *J. Mol. Biol.* **296**, 633–649 (2000). Medline doi:10.1006/jmbi.1999.3475
14. O. Pornillos, B. K. Ganser-Pornillos, B. N. Kelly, Y. Hua, F. G. Whitby, C. D. Stout, W. I. Sundquist, C. P. Hill, M. Yeager, X-ray structures of the hexameric building block of the HIV capsid. *Cell* **137**, 1282–1292 (2009). Medline doi:10.1016/j.cell.2009.04.063
15. S. Du, L. Betts, R. Yang, H. Shi, J. Concel, J. Ahn, C. Aiken, P. Zhang, J. I. Yeh, Structure of the HIV-1 full-length capsid protein in a conformationally trapped unassembled state induced by small-molecule binding. *J. Mol. Biol.* **406**, 371–386 (2011). Medline doi:10.1016/j.jmb.2010.11.027
16. O. Pornillos, B. K. Ganser-Pornillos, M. Yeager, Atomic-level modelling of the HIV capsid. *Nature* **469**, 424–427 (2011). Medline doi:10.1038/nature09640
17. G. Zhao, J. R. Perilla, E. L. Yufenyuy, X. Meng, B. Chen, J. Ning, J. Ahn, A. M. Gronenborn, K. Schulten, C. Aiken, P. Zhang, Mature HIV-1 capsid structure by cryo-electron microscopy and all-atom molecular dynamics. *Nature* **497**, 643–646 (2013). Medline doi:10.1038/nature12162
18. I. J. Byeon, X. Meng, J. Jung, G. Zhao, R. Yang, J. Ahn, J. Shi, J. Concel, C. Aiken, P. Zhang, A. M. Gronenborn, Structural convergence between Cryo-EM and NMR reveals intersubunit interactions critical for HIV-1 capsid function. *Cell* **139**, 780–790 (2009). Medline doi:10.1016/j.cell.2009.10.010
19. B. K. Ganser-Pornillos, A. Cheng, M. Yeager, Structure of full-length HIV-1 CA: A model for the mature capsid lattice. *Cell* **131**, 70–79 (2007). Medline doi:10.1016/j.cell.2007.08.018
20. Y. Aida, H. Murakami, M. Takahashi, S. N. Takeshima, Mechanisms of pathogenesis induced by bovine leukemia virus as a model for human T-cell leukemia virus. *Front Microbiol* **4**, 328 (2013). Medline doi:10.3389/fmicb.2013.00328
21. N. Gillet, A. Florins, M. Boxus, C. Burteau, A. Nigro, F. Vandermeers, H. Balon, A. B. Bouzar, J. Defoiche, A. Burny, M. Reichert, R. Kettmann, L. Willems, Mechanisms of leukemogenesis induced by bovine leukemia virus: Prospects for novel anti-retroviral therapies in human. *Retrovirology* **4**, 18 (2007). Medline doi:10.1186/1742-4690-4-18
22. S. M. Rodríguez, A. Florins, N. Gillet, A. de Brogniez, M. T. Sánchez-Alcaraz, M. Boxus, F. Boulanger, G. Gutiérrez, K. Trono, I. Alvarez, L. Vagnoni, L. Willems, Preventive and therapeutic strategies for bovine leukemia virus: Lessons for HTLV. *Viruses* **3**, 1210–1248 (2011). Medline doi:10.3390/v3071210
23. M. Fujii, M. Matsuoka, in *Fields Virology*, D. M. Knipe, P. M. Howley, Eds. (Wolters Kluwer/Lippincott Williams & Wilkins Health, Philadelphia, PA, 2013), vol. 2, chap. 48, pp. 1474–1501.
24. Materials and methods are available as supplementary materials on *Science* Online.
25. G. Cardone, J. G. Purdy, N. Cheng, R. C. Craven, A. C. Steven, Visualization of a missing link in retrovirus capsid assembly. *Nature* **457**, 694–698 (2009). Medline doi:10.1038/nature07724
26. D. K. Worthylake, H. Wang, S. Yoo, W. I. Sundquist, C. P. Hill, Structures of the HIV-1 capsid protein dimerization domain at 2.6 A resolution. *Acta Crystallogr. D Biol. Crystallogr.* **55**, 85–92 (1999). Medline doi:10.1107/S0907444998007689
27. A. T. Gres, K. A. Kirby, V. N. KewalRamani, J. J. Tanner, O. Pornillos, S. G. Sarafianos, X-ray crystal structures of native HIV-1 capsid protein reveal conformational variability. *Science* (2015); doi:10.1126/science.aaa5936
28. K. Chen, G. Piszczek, C. Carter, N. Tjandra, The maturational refolding of the β-hairpin motif of equine infectious anemia virus capsid protein extends its helix α1 at capsid assembly locus. *J. Biol. Chem.* **288**, 1511–1520 (2013). Medline

doi:10.1074/jbc.M112.425140
29. M. Obr, R. Hadravová, M. Doležal, I. Křížová, V. Papoušková, L. Zídek, R. Hrabal, T. Ruml, M. Rumlová, Stabilization of the β-hairpin in Mason-Pfizer monkey virus capsid protein- a critical step for infectivity. *Retrovirology* **11**, 94 (2014). Medline doi:10.1186/s12977-014-0094-8
30. I. Gross, H. Hohenberg, C. Huckhagel, H. G. Kräusslich, N-Terminal extension of human immunodeficiency virus capsid protein converts the in vitro assembly phenotype from tubular to spherical particles. *J. Virol.* **72**, 4798–4810 (1998). Medline
31. A. J. Price, D. A. Jacques, W. A. McEwan, A. J. Fletcher, S. Essig, J. W. Chin, U. D. Halambage, C. Aiken, L. C. James, Host cofactors and pharmacologic ligands share an essential interface in HIV-1 capsid that is lost upon disassembly. *PLOS Pathog.* **10**, e1004459 (2014). Medline doi:10.1371/journal.ppat.1004459
32. H. Yang, X. Ji, G. Zhao, J. Ning, Q. Zhao, C. Aiken, A. M. Gronenborn, P. Zhang, Y. Xiong, Structural insight into HIV-1 capsid recognition by rhesus TRIM5α. *Proc. Natl. Acad. Sci. U.S.A.* **109**, 18372–18377 (2012). Medline doi:10.1073/pnas.1210903109
33. F. van den Ent, J. Löwe, RF cloning: A restriction-free method for inserting target genes into plasmids. *J. Biochem. Biophys. Methods* **67**, 67–74 (2006). Medline doi:10.1016/j.jbbm.2005.12.008
34. W. Kabsch, Integration, scaling, space-group assignment and post-refinement. *Acta Crystallogr. D Biol. Crystallogr.* **66**, 133–144 (2010). Medline doi:10.1107/S0907444909047374
35. P. R. Evans, G. N. Murshudov, How good are my data and what is the resolution? *Acta Crystallogr. D Biol. Crystallogr.* **69**, 1204–1214 (2013). Medline doi:10.1107/S0907444913000061
36. T. R. Schneider, G. M. Sheldrick, Substructure solution with SHELXD. *Acta Crystallogr. D Biol. Crystallogr.* **58**, 1772–1779 (2002). Medline doi:10.1107/S0907444902011678
37. G. Bricogne, C. Vonrhein, C. Flensburg, M. Schiltz, W. Paciorek, Generation, representation and flow of phase information in structure determination: Recent developments in and around SHARP 2.0. *Acta Crystallogr. D Biol. Crystallogr.* **59**, 2023–2030 (2003). Medline doi:10.1107/S0907444903017694
38. J. P. Abrahams, A. G. Leslie, Methods used in the structure determination of bovine mitochondrial F1 ATPase. *Acta Crystallogr. D Biol. Crystallogr.* **52**, 30–42 (1996). Medline doi:10.1107/S0907444995008754
39. G. Bricogne *et al*., BUSTER (Global Phasing Ltd., Cambridge, UK, 2009).
40. P. Emsley, B. Lohkamp, W. G. Scott, K. Cowtan, Features and development of Coot. *Acta Crystallogr. D Biol. Crystallogr.* **66**, 486–501 (2010). Medline doi:10.1107/S0907444910007493
41. A. J. McCoy, R. W. Grosse-Kunstleve, P. D. Adams, M. D. Winn, L. C. Storoni, R. J. Read, Phaser crystallographic software. *J. Appl. Crystallogr.* **40**, 658–674 (2007). Medline doi:10.1107/S0021889807021206
42. P. V. Afonine, R. W. Grosse-Kunstleve, N. Echols, J. J. Headd, N. W. Moriarty, M. Mustyakimov, T. C. Terwilliger, A. Urzhumtsev, P. H. Zwart, P. D. Adams, Towards automated crystallographic structure refinement with *phenix.refine*. *Acta Crystallogr. D Biol. Crystallogr.* **68**, 352–367 (2012). Medline doi:10.1107/S0907444912001308
43. R. Das, D. Baker, Macromolecular modeling with Rosetta. *Annu. Rev. Biochem.* **77**, 363–382 (2008). Medline doi:10.1146/annurev.biochem.77.062906.171838
44. P. D. Adams, P. V. Afonine, G. Bunkóczi, V. B. Chen, I. W. Davis, N. Echols, J. J. Headd, L. W. Hung, G. J. Kapral, R. W. Grosse-Kunstleve, A. J. McCoy, N. W. Moriarty, R. Oeffner, R. J. Read, D. C. Richardson, J. S. Richardson, T. C. Terwilliger, P. H. Zwart, PHENIX: A comprehensive Python-based system for macromolecular structure solution. *Acta Crystallogr. D Biol. Crystallogr.* **66**, 213–221 (2010). Medline doi:10.1107/S0907444909052925
45. P. R. Evans, An introduction to data reduction: Space-group determination, scaling and intensity statistics. *Acta Crystallogr. D Biol. Crystallogr.* **67**, 282–292 (2011). Medline doi:10.1107/S090744491003982X
46. J. E. Padilla, T. O. Yeates, A statistic for local intensity differences: Robustness to anisotropy and pseudo-centering and utility for detecting twinning. *Acta Crystallogr. D Biol. Crystallogr.* **59**, 1124–1130 (2003). Medline doi:10.1107/S0907444903007947
47. M. D. Winn, C. C. Ballard, K. D. Cowtan, E. J. Dodson, P. Emsley, P. R. Evans, R. M. Keegan, E. B. Krissinel, A. G. Leslie, A. McCoy, S. J. McNicholas, G. N. Murshudov, N. S. Pannu, E. A. Potterton, H. R. Powell, R. J. Read, A. Vagin, K. S. Wilson, Overview of the CCP4 suite and current developments. *Acta Crystallogr. D Biol. Crystallogr.* **67**, 235–242 (2011). Medline doi:10.1107/S0907444910045749
48. W. Kabsch, A discussion of the solution for the best rotation to relate two sets of vectors. *Acta Crystallogr. A* **34**, 827–828 (1978). doi:10.1107/S0567739478001680
49. R. L. Kingston, T. Fitzon-Ostendorp, E. Z. Eisenmesser, G. W. Schatz, V. M. Vogt, C. B. Post, M. G. Rossmann, Structure and self-association of the Rous sarcoma virus capsid protein. *Structure* **8**, 617–628 (2000). Medline doi:10.1016/S0969-2126(00)00148-9
50. C. Tang, Y. Ndassa, M. F. Summers, Structure of the N-terminal 283-residue fragment of the immature HIV-1 Gag polyprotein. *Nat. Struct. Biol.* **9**, 537–543 (2002). Medline
51. V. B. Chen, W. B. Arendall 3rd, J. J. Headd, D. A. Keedy, R. M. Immormino, G. J. Kapral, L. W. Murray, J. S. Richardson, D. C. Richardson, MolProbity: All-atom structure validation for macromolecular crystallography. *Acta Crystallogr. D Biol. Crystallogr.* **66**, 12–21 (2010). Medline doi:10.1107/S0907444909042073

ACKNOWLEDGMENTS

The crystal structures (model coordinates and structure factors) are available in the Protein Data Bank under accession codes 4PH0, 4PH1, 4PH2, and 4PH3. We acknowledge funding from CNRS (France, program LIA 316), ANII (Uruguay), CeBEM (www.cebem.org.ar) and FOCEM (MERCOSUR Structural Convergence Fund, COF 03/11). We thank P. Guardado-Calvo and T. Krey for helpful comments. We acknowledge the Recombinant Proteins Unit (Institut Pasteur de Montevideo) for the access to protein expression and purification facilities. Thanks to A. Lebedev for tailor-made programs to analyze NCS and B. Guimaraes at beamline Proxima 1 (synchrotron Soleil) for assistance with full-length CA data collection. We want to thank F. Rey for the lively discussions.

SUPPLEMENTARY MATERIALS

www.sciencemag.org/cgi/content/full/science.aaa5182/DC1
Materials and Methods
Figs. S1 to S8
Tables S1 and S2
References (*33*–*51*)

2 January 2015; accepted 10 April 2015
Published online 4 June 2015
10.1126/science.aaa5182

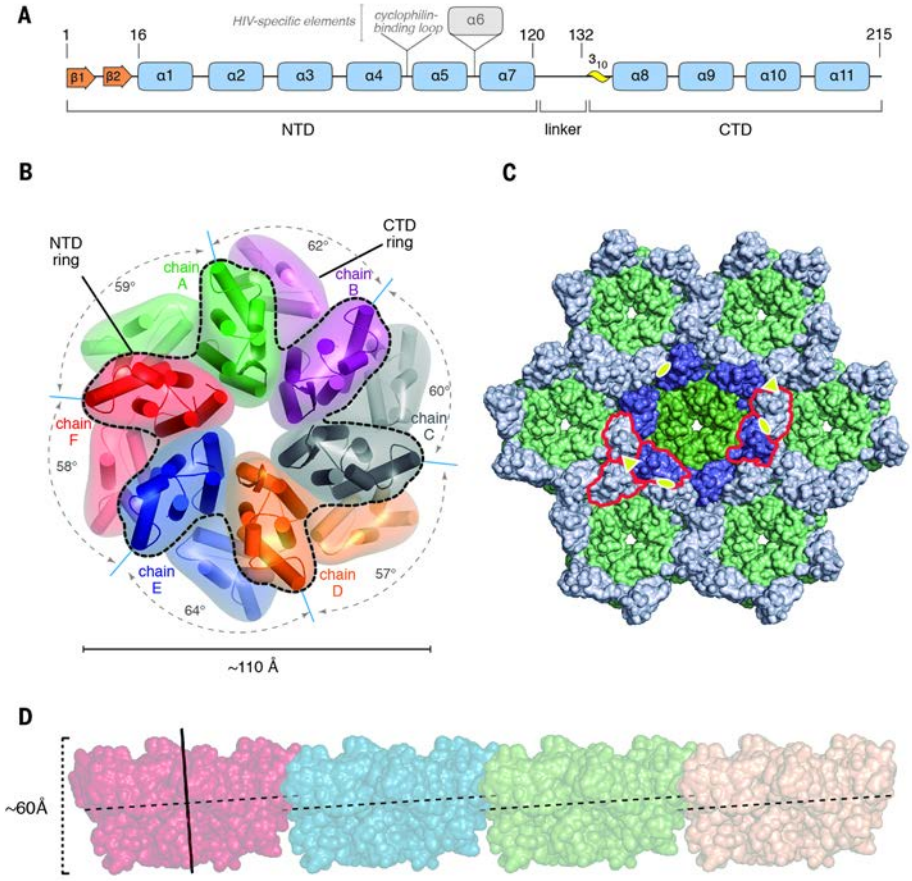

Fig. 1. Structure of BLV CA and crystal packing. (**A**) Linear representation of BLV CA with numbered secondary structure elements. Domain boundaries and missing segments found in HIV-1 CA are indicated. (**B**) Schematic representation of the contents of the asymmetric unit of mature BLV CA crystals, corresponding to a hexameric unit. Each protomer is depicted in a different color. The ring of NTDs is outlined and angles between centers of mass of neighbor NTD pairs are indicated. (**C**) Solvent accessible surface of seven interacting hexameric units, forming a pseudo-hexagonal planar array. The central hexamer is highlighted with darker tones, and the two colors distinguish NTDs (green) from CTDs (blue). In this orientation the CTD rings are shown closer to the reader. Independent Q2 (yellow ovals) and Q3 (yellow triangles) axes are highlighted, and interacting CTDs at selected Q2 and Q3 interfaces, outlined (further details in fig. S5). (**D**) Tiled organization of successive hexameric building units in the crystal. The 2D lattice plane is horizontal in this view. The quasi-6-fold non-crystallographic axis is shown as a black stick on the left-most hexamer. The dashed lines (perpendicular to the Q6 axes) connect identical positions of different protomers within the hexamers, highlighting the approximately 10% vertical translational shift in certain adjacent interfaces.

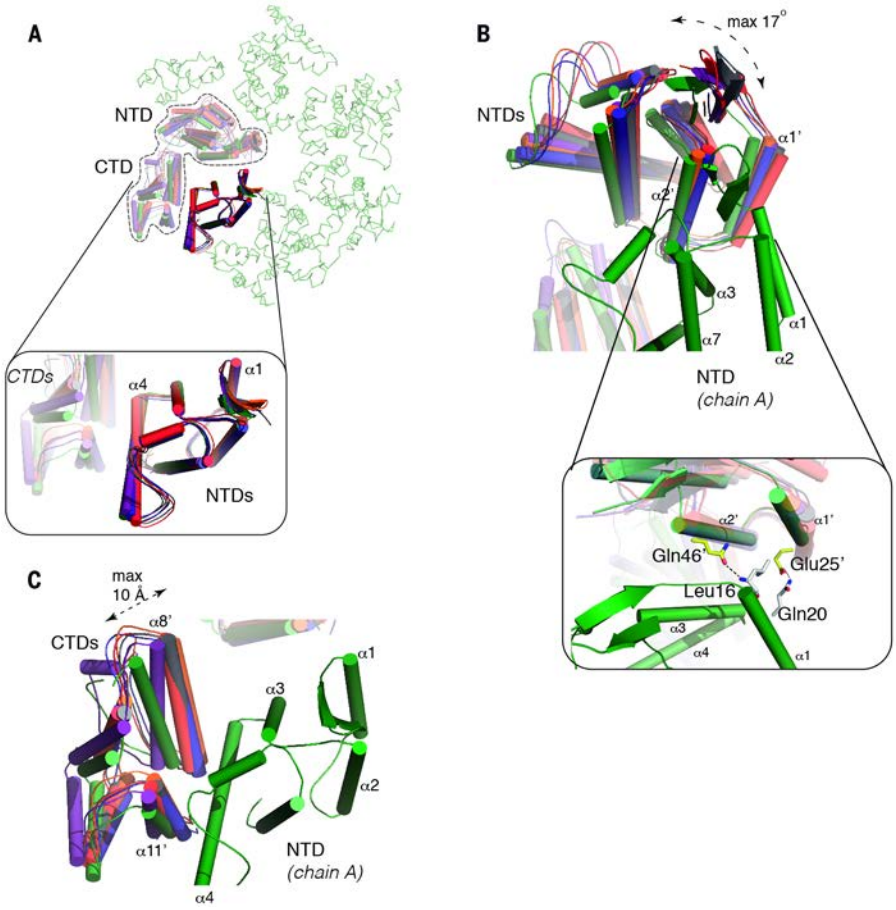

Fig. 2. Variations among intra-hexamer contacts. (**A**) The hexamer is shown as a green transparent ribbon. One protomer is outlined for reference. The N-terminal domains (NTDs) of the six chains (solid cartoons, colored as in Fig. 1B) were superposed onto protomer A. The resulting rotated positions of neighboring subunits are shown in semitransparent cartoon. The inset highlights the good superposition among all NTDs (0.5 to 0.6 Å rmsd) (**B**) The view in (A) is rotated by approximately 45° along a horizontal axis. Only one of the superposed NTDs is shown in green (chain A), with neighboring NTDs colored by chain and α-helix labels identified with a prime. Large variations among different inter-protomer NTD-NTD interfaces are observed (maximum angular shift observed between chains A and F is labeled). The inset shows a close-up, with residues (in sticks) involved in H-bonds in all the inter-protomer pairs. (**C**) The same NTD is shown as a green cartoon (chain A), same orientation as panel (A). CTD-CTD interactions are highlighted, revealing important variation of CTD-CTD interfaces. The dashed arrow highlights the maximum shift observed between helices α8 of chains A and D.

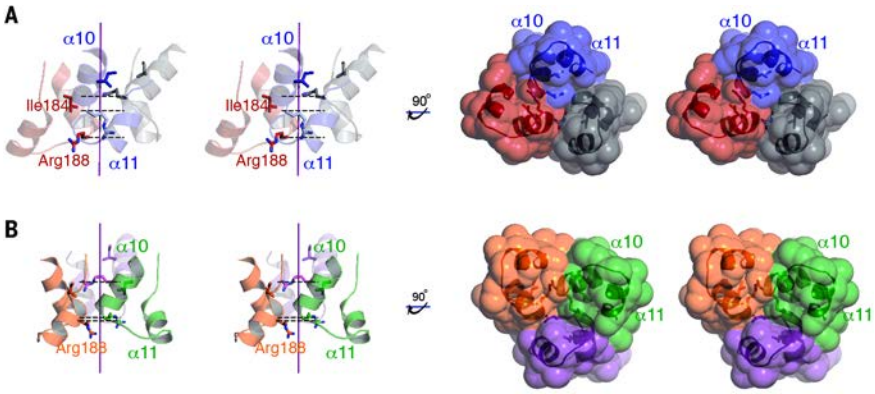

Fig. 3. Close-up of the two independent trimeric interfaces stabilizing the BLV CA lattice, as observed in the crystal asymmetric unit. Stereo views of two orthogonal orientations of the interface between (**A**) protomers B/D/F and (**B**) protomers A/C/E, from three neighbor hexamers, are shown. Chains colored as in Fig. 1B. On the left panels, side-views with respect to the quasi-3-fold axes (depicted as purple sticks). The positions of R188 Cα atoms (dashed lines), highlight variable height shifts among the interacting protomers. R188 and I184 (on the same side of α10) are shown as sticks for reference. On the right, solvent accessible surface representations show the close contacts among the three interacting protomers.